Published in IET Radar, Sonar and Navigation
Received on 20th February 2009
Revised on 23rd July 2009
doi: 10.1049/iet-rsn.2009.0031

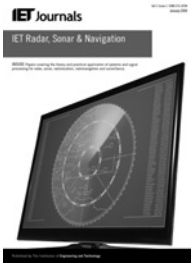

ISSN 1751-8784

Stealth technology for wind turbines

J. Pinto J.C.G. Matthews G.C. Sarno

Sensor Systems Department, BAE SYSTEMS Advanced Technology Centre, West Hanningfield Road, Gt. Baddow, Chelmsford, Essex CM2 8HN, UK
E-mail: jon.pinto@baesystems.com

Abstract: Currently, a large proportion of proposed UK wind farms have either concerns raised at the pre-planning stage or formal objections made by radar operators on the basis of the potential for wind turbines to cause interference to radar systems. The current generation of on and off-shore three-bladed horizontal axis wind turbines have radar signatures consistent with their often very large physical size and hence considerable potential to reduce the ability of ground-based radars to detect targets in the vicinity of the farm. The impact of wind farms, particularly on ground-based aviation radars such as those operated for air defence and military and civil air traffic control purposes is likely to become particularly acute as European Union member governments strive to meet the requirements for energy generation under the Renewables Obligation. In addition, the increasing number of offshore wind farm projects proposed has the potential to cause interference to marine radars such as coastal vessel traffic services and those on-board vessels for navigational purposes. This study considers the options available for the reduction of turbine radar signature and presents solutions for each of the main external turbine components. The radar signature reduction approaches are based on existing technologies developed for aerospace stealth applications. However, the realisation of these for the purposes of reducing wind turbine radar signatures is a novel development, particularly in the solutions proposed. The reduction of wind turbine-induced radar interference is a growing area of research.

1 Introduction

A number of mitigation techniques are being considered to reduce the impact of wind turbines on radars [8–13]. Post-processing techniques have the potential to render 'victim' radars less susceptible to returns from turbines, and 'gap fillers' reduce the area around farms in which targets cannot be detected. Sensitivity reduction in the direction of the farm for fixed radar installations is also being considered by antenna modification, antenna tilting, physical obscuration techniques such as radar absorbent material (RAM) fences and modification of the layout of turbines within farms to better fit into clutter map cells of some radar types. Radar signature reduction of the wind turbines themselves has the potential to benefit all radar systems, marine and aviation, and is likely to form an important part of the overall solution to the radar–wind farm interaction problem, and it is this area on which this paper reports.

The majority of aviation and marine radars can be considered as operating over two frequency bands, 2.7–3.1 and 9.1–9.41 GHz. The former encompasses the bulk of modern air defence (AD) radars, military and civil air traffic control (ATC) terminal approach and primary surveillance radars (PSR) and a proportion of marine vessel traffic services (VTS) and long range marine navigation radars associated with larger vessels.

X-band radars within the latter frequency range are predominantly associated with the marine environment, these frequencies typically encompassing marine navigation radars on smaller craft and further VTS operated by port authorities.

A Vestas V82 2MW turbine was used as a case study for prediction of the monostatic radar cross-section (RCS) of a turbine in these key frequency bands. The turbine was divided into the main external components, the tower, blades, nacelle and nosecone, and signature reduction approaches developed for each. These were then brought together and an estimate made of the overall signature reduction which can be achieved. The reduction techniques

used were not specific to the V82 turbine and the solutions developed were intended to be applicable with minor modification to the majority of the current generation of on and off-shore wind generating capacity.

The radar impact of a wind farm comprised first of the V82's, and then reduced RCS turbines, was considered by putting these signatures into a combined system model developed in-house. This 'AEOLUS' code encompassed ATC PSR performance, radar to wind-farm terrain propagation effects and the RCS of individual wind turbines and their layout within the farm using aspect-dependent coherent summation. RCS prediction is described in Section 2 whereas reduction techniques and the impact of the untreated and reduced RCS turbines in a wind farm on the ability of a radar to detect an air vehicle in the vicinity of the farm is considered in Sections 3 and 4.

2 Turbine RCS estimation

The Vestas V82 turbine is typical in its design and construction of the current generation of on- and off-shore wind turbines with a 40 m blade length and 78 m tower height. CAD geometry of the main components was used to derive RCS estimates for each and subsequently for the turbine as a whole. The in-house prediction code MITRE [1], based on the method of physical optics (PO), was used to determine the 3 and 10 GHz monostatic co-polar RCS of the structures, the results being compared with commercial codes at lower frequencies where the problem is electrically smaller.

Peak values for the whole turbine were found to be around 501 200 m^2 at 3 GHz, or +57 dBsm presented in decibel square metres as is conventional, rising to +62 dBsm at 10 GHz as the structure became electrically larger. The predicted overall turbine RCS at 3 GHz is shown as a function of blade rotation angle in Fig. 2 for energy incident from the positive x-axis, and in Fig. 3 for the case where the illumination angle is co-incident with the positive y-axis (with the blades rotating towards and away from the viewer). The co-ordinate system used for the modelling is represented schematically in Fig. 1. The face of the blades on the V82 and other horizontal axis turbines is tilted back by an angle of approximately 5° and hence

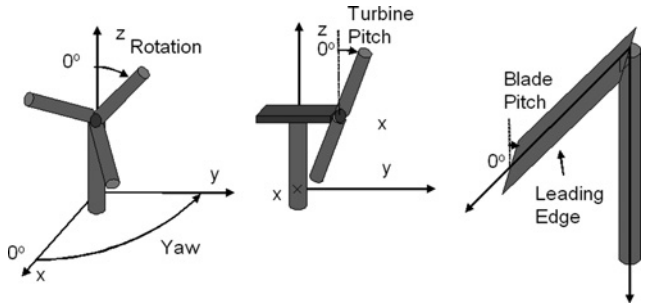

Figure 1 *Wind turbine geometry co-ordinate system*

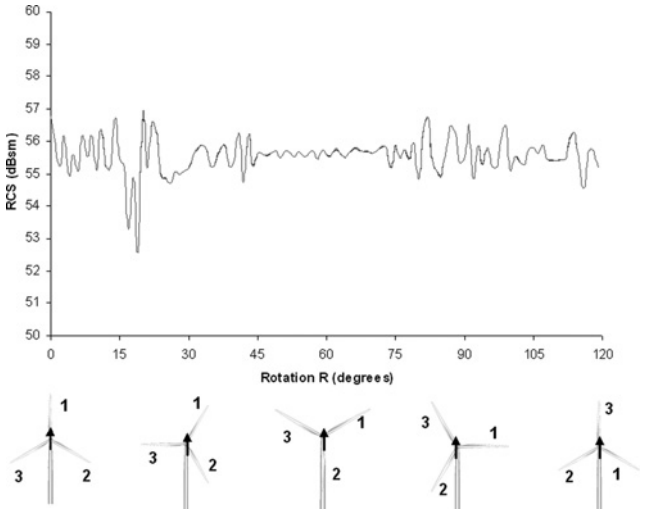

Figure 2 *Monostatic RCS of V82 turbine as a function of blade rotation angle for a frequency of 3 GHz, illumination from the positive x-direction*

the direction of incident energy cannot strictly be referenced in terms of parallel and perpendicular to the plane of blade rotation for horizontal incidence.

Considering Fig. 2, the RCS varies with blade rotation as the blades shadow the tower at certain rotation angles. The blades themselves are not symmetrical when observed in cross-section; rather the leading edge exhibits a much larger radius than the trailing. Consequently, the 30° rotation case in Fig. 2 does not yield quite the same RCS as that for 90°.

As might be anticipated for such an electrically large structure (~1000 λ at 3 GHz) the impact of diffraction terms and polarisation-sensitive effects were found to be small and thus are not presented here for brevity. The vast majority of the scattering was found to be attributable to specular returns. Further detail relating to the contribution from second-order effects and comparison of the results with other prediction tools has already been reported and is given in [2]. Fig. 3 shows that the RCS is largely independent of blade rotation when the turbine is illuminated from this aspect angle, the RCS being dominated by returns from the tower.

Turbine towers are typically manufactured from concrete or rolled steel, the latter being the more commonplace. The V82 tower is manufactured from seam welded rolled steel sections typically 20–40 mm in wall thickness, with bulkheads between sections to enable them to be bolted together at the wind farm site. The lower portion consists of a 3.65 m diameter cylinder, 54.3 m in height on top of which sits a 23.2 m high truncated cone with a diameter at the uppermost point of 2.3 m. The dimensions are summarised in Fig. 4.

According to the method of PO, the RCS of the tower, because of specular scattering, may be estimated from the

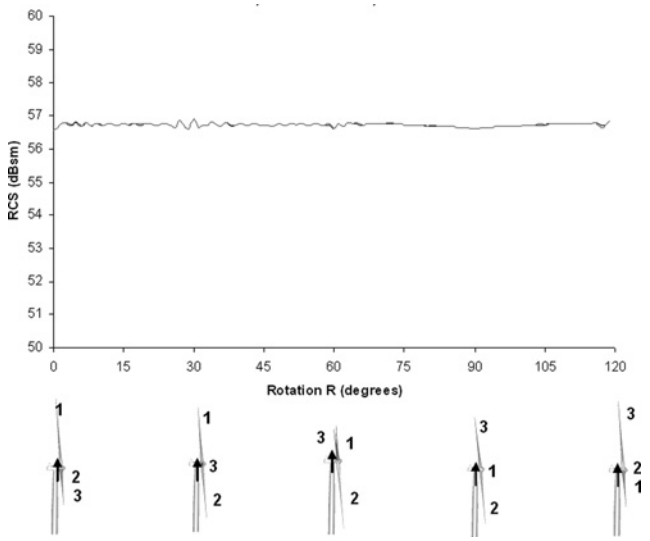

Figure 3 *Monostatic RCS of V82 turbine as a function of blade rotation angle for a frequency of 3 GHz, illumination from the positive y-direction*

extent of a region termed the stationary phase zone associated with each geometric component from which the tower may be considered to be formed. Over this region the phase variation is less than $\lambda/8$ and scattering is therefore assumed to be coherent. In the case of returns from the lower cylindrical section, this simply derived kaL^2 estimate is widely reported in the literature [3], where k is the free space wave number, a the radius and L the length. The approximations only hold for cases where the direction of propagation is normal to the long axis of the cylinder, the conductivity is sufficiently high to allow the surface to be regarded as a perfect electrical conductor (PEC) and the turbines are themselves in the far-field of the radiating

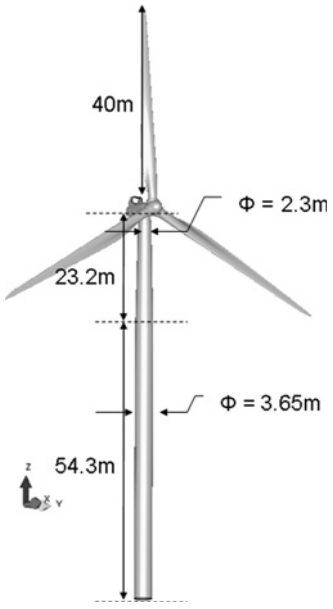

Figure 4 *Turbine tower geometry showing cylindrical section beneath a truncated cone*

aperture. In the case of the tower as a whole, this corresponds to a $2D^2/\lambda$ separation of 120 km at 3 GHz, where D is the diameter of the aperture over which the phase front is being considered, in this case the 78 m tower height. This is comparable with the maximum operational range of some AD and ATC radars and therefore this criterion, in practice, may not necessarily be fulfilled. The variation in phase of the illuminating radiation, over the length of the tower, differs by more than $\lambda/8$ if the radar to turbine down-range distance is less than this figure. This criterion is generally regarded as an acceptable approximation to the far-field condition; however, for any target of significant size, illuminated by a point source at a finite distance, the phase front of the illuminating radiation remains curved and only an approximation to the true far-field condition. Under this circumstance, the perceived RCS is generally less than the far-field values shown in Figs. 2 and 3, the effect increasing as the range is reduced. The work presented does not seek to investigate this effect as presented, although near-field predictions were completed as part of the work for specific radar–wind farm case studies, but instead is confined to far-field RCS reductions.

The frequency and slope angle-dependent RCS of the conical section may be obtained by division into N slices, each of length $l = L/N$, where L is the vertical height [4]

$$\sigma = \left[\sum_{n=1}^{N}\sqrt{\left[\frac{2\pi}{\lambda}\left(\frac{r_2 - r_1}{N-1}\right)(n-1) + r_1\right]}\frac{L}{N} \times \cos\theta\frac{\sin\left((2\pi/\lambda)L\sin\theta\right)}{(2\pi/\lambda)L\sin\theta}e^{4i\pi/\lambda((r_2-r_1)/(N-1))}\right]^2 \quad (1)$$

The slope angle (in radians) is given by θ, and r_1 and r_2 are the smaller and larger radii, respectively. Substitution of the dimensions given previously yields 3 GHz RCS estimates of 55.3 dBsm (338 332 m^2) for the cylindrical portion and only 14.0 dBsm (28 m^2) for the conical section. The non-coherent sum is therefore dominated by the cylindrical section and rises from 55.3 dBsm at 3 GHz to 60.5 dBsm at 10 GHz, which may be compared with the 55.5 and 60.7 dBsm obtained from the MITRE PO code. Approximately 75% of the overall turbine RCS, varying to some extent with blade and nacelle orientation, is derived from the tower in the far-field case.

The blades were found to be the next most significant source of scatter, constituting a total of around 15% (5% each) of the overall turbine RCS. The peak blade RCS was estimated using the MITRE PO code to be ~40 dBsm at 3 GHz rising to ~45 dBsm at 10 GHz. Since the blades are already shaped for aerodynamic reasons, the use of shaping as a means of RCS reduction is not practicable. V82 turbine blades are of composite construction using a resin infusion process and hence the entirety of the blade cross-section forms part of the supporting structural

doi: 10.1049/iet-rsn.2009.0031

material. In addition, around two-thirds of the blade is covered with a fine lightning strike protective mesh just beneath the outer surface. For the purposes of RCS prediction, this allowed the blade to be treated as a PEC material.

The nacelle is a composite housing providing environmental protection to the generator and gearbox. In the case of the V82, it is manufactured using a wet lay-up process incorporating chopped strand mat in a polyester resin. The wall thickness is around 13 mm and the structure is partially transparent to microwave radiation over the frequency ranges being considered. Neglecting any scattering from the generator, the monostatic RCS of the V82 nacelle is substantially lower than either the tower or blades for the majority of illumination angles, typically <10 dBsm. However, the large planar sides particular to this design do generate significant broadside flashes up to around 50 dBsm. The nosecone was also found to be significantly lower in RCS than the other components (maximum of 17 dBsm if assumed to be PEC) and so was unlikely to become the dominant scatterer unless very large RCS reductions were achieved elsewhere.

3 RCS reduction approaches

As the dominant scatterer, the tower was addressed first. An effective RAM solution giving a 20 dBsm reduction in both bands was developed for application to the outer surface but this was later superseded by shaping. RAM had the benefit that it could be applied to existing structures but the disadvantages of increased cost and weight, and the need to qualify the material to withstand the sometimes harsh environments in which wind turbines operate. Instead, the cylinder and truncated cone of the existing V82 tower were replaced by a single conical structure. As the cone angle is varied from the cylindrical case, $\theta = 0^\circ$, the discontinuities in induced currents in the stationary phase zone caused by the ends, result in a characteristic side-lobe pattern, each side lobe having half the width of the main. The lobe width varies inversely with cone electrical length. Having maintained the truncated cone upper diameter (fixed because of the need to mate to the nacelle), the lower diameter and so cone angle was varied. The side-lobe structure as a function of cone base diameter and hence slope angle, at a frequency of 3 GHz, is shown in Fig. 5, based on (1).

The MITRE PO model [1] was also used to investigate the optimum cone angle. Given the relatively long run times and fine structure associated with the side-lobe pattern, particularly at higher frequencies, the number of prediction runs feasible resulted in an under-sampled side-lobe representation, which is shown in Fig. 6. The dotted line represents the RCS of a cone with the same top and base diameters as the V82 turbine but formed from a single truncated cone, this being less than optimal.

By inspection of Figs. 5 and 6, and conversion from base diameter to slope angle, it is possible to find angles where minima occur at the centre frequencies of both bands of interest. For the V82 geometry, such a minima was found to occur at 0.6°, corresponding to a base diameter of 3.9 m. The 4.15 m limit is dictated by the need to transport the tower sections by road.

The predicted RCS in both bands could theoretically be reduced by up to 43 dBsm using this approach. The use of side-lobe minima, rather than just the side-lobe envelope can allow very large reductions to be realised. However, in practice, particularly in the high band, the variation in frequency over the band results in a shift in the position of these minima. Consequently, although selection of a cone

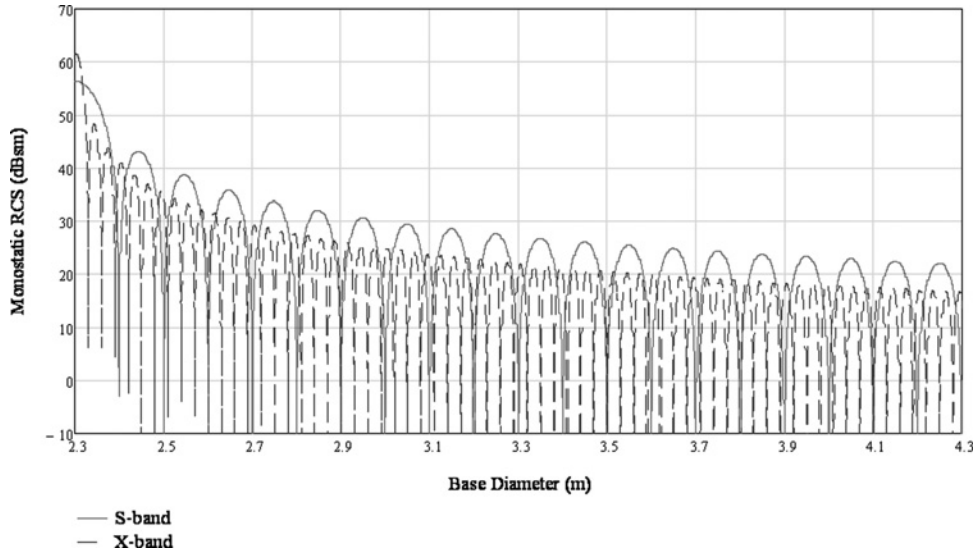

Figure 5 *RCS of truncated conical tower structure showing side-lobe component of specular scattering with base diameter and so cone angle for a fixed upper diameter of 2.3 m*

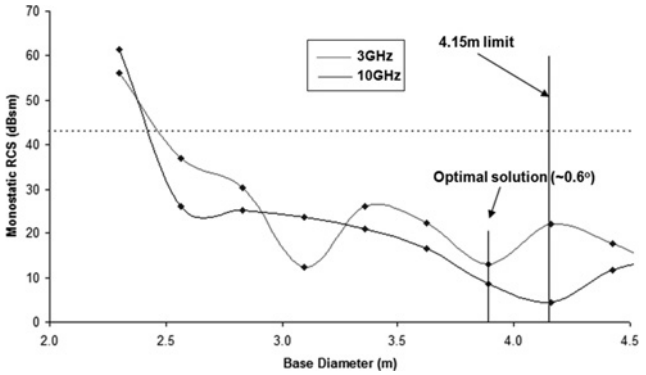

Figure 6 *RCS as a function of cone base diameter for 3 and 10 GHz*

angle corresponding to minima at the centre frequencies of both bands would be prudent, not all of the benefit is likely to be realised in practice. This approach also assumes that the radar is at a similar height to the turbine above mean sea level and does not consider the apparent elevation because of the curvature of the Earth. Nonetheless, the technique is effective as a means of reducing the far-field RCS. Careful consideration of these factors is required to ensure that tower shaping is implemented correctly.

For the case of onshore wind farms, turbines are typically situated on high ground in order to capture maximum wind energy and hence sloping of the tower remains practical. However, additional care might be required if the turbines were intended to be installed offshore where a radar to turbine 'look-down' angle might exist. The main lobe associated with backscatter from the modified V82 tower, sloped at 0.6°, was found to occupy an angular range of slightly less than 0.1° at 3 GHz. Radars at an elevation angle of between 0.55 and 0.65° would hence be in the main lobe of backscattered tower radiation, neglecting the curvature of the Earth. The effective height of the bottom of the main lobe (at 0.55°) is given in Table 1 as a function of range from the turbine. The table takes the curvature of the Earth into account but does not consider any anomalous propagation effects.

In the case of the blades, two structural RAM solutions were developed. A modified Salisbury screen-based absorber was developed for incorporation into the leading and trailing edge regions whereas a circuit analogue (CARAM)-based design was developed for the mid-blade region with tighter constraints on thickness and mass. The complex relative permittivity of the resin-glass material from which the outer regions of the blade were fabricated was measured to be 4.59−0.004i, whereas the relatively thick blade paint layer was found to be 2.81−0.006i (X-band mean). The resin-glass material parameters were measured by producing a number of 2′ square laminate sheets and characterising their scattering parameters using a quasi-optical free space focused Gaussian beam measurement system in order to minimise any variation associated with changes in fibre volume fraction. The thin paint layer was characterised using the same equipment by depositing the material on a thin impermeable carrier (typically 50 μm thick Kapton film). The paint layer was then represented as a normalised lumped admittance. The Salisbury screen-based RAM design is shown schematically in Fig. 7. The CARAM-based build has been omitted because of commercial sensitivities, although the reflection loss performance was similar to that of the Salisbury screen reported here. A good general review of commercially available RAM is given in [3].

The V82 aluminium lightning mesh was removed and replaced with two meshes, as shown. The upper 'coarse' mesh was essentially transparent to microwave radiation in both bands whereas the lower formed a ground plane. In this way, resistance to lightning strike may be preserved

Table 1 Height of bottom of 3 GHz main lobe scatter from turbine tower, with effect of Earth curvature considered

Range from scatterer, m	Curved earth angle, deg	Curved earth height effect, m	Flat earth height of main lobe minima, m	Curved earth height of main lobe minima, m
0	0	0	0	0
10 000	0.090	7.81	96	88
20 000	0.179	31.25	192	161
30 000	0.269	70.31	288	218
40 000	0.358	125.00	384	259
50 000	0.448	195.30	480	285
60 000	0.537	281.23	576	295
70 000	0.627	382.78	672	289
80 000	0.716	499.94	768	268
90 000	0.806	632.72	864	231

doi: 10.1049/iet-rsn.2009.0031

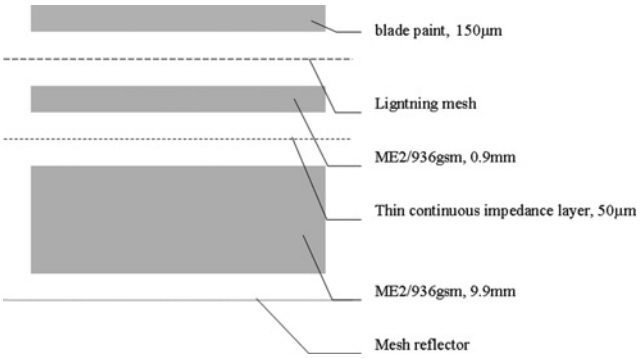

Figure 7 *Build of Salisbury screen-based blade absorber*

with the 'lossy' RAM layer sandwiched between the two conductive grids. Several trial panels were manufactured in order to demonstrate the viability of the solution. Fig. 8 shows the manufacture of a typical test panel.

The normal incidence reflection loss measured using a bistatic arch is shown against prediction in Fig. 9. The first harmonic was made to shift to lower frequencies (into the upper band) by the addition of significant capacitive reactance to the active layer, which was characterised as a normalised lumped admittance.

Hence the structural Salisbury screen-based RAM developed is novel in respect of including a lightning protection mechanism which does not impact significantly on the electrical properties of the structure and by the use of a thin sheet impedance layer with a carefully controlled capacitive reactance. The latter achieves maximum reflection losses in both bands by manipulating the frequency of the X-band resonance to correspond with the particular band of interest which maintaining the position of the S-band absorption minima. Using this approach, reductions of the order of 15 dBsm were demonstrated for both frequency bands of interest, reducing the peak RCS of the blades to 25 dBsm at 3 GHz and 30 dBsm at 10 GHz.

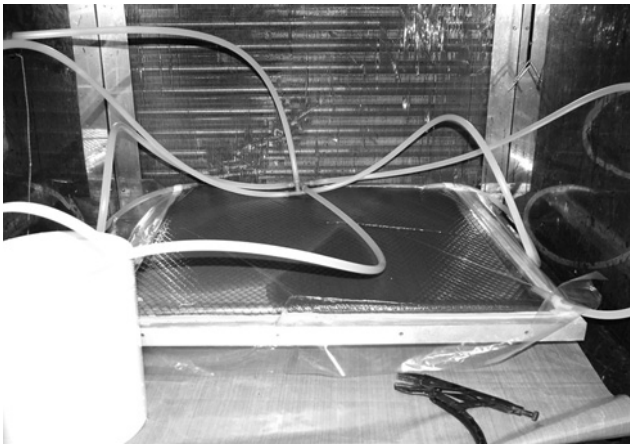

Figure 8 *Resin infusion of a blade test panel*

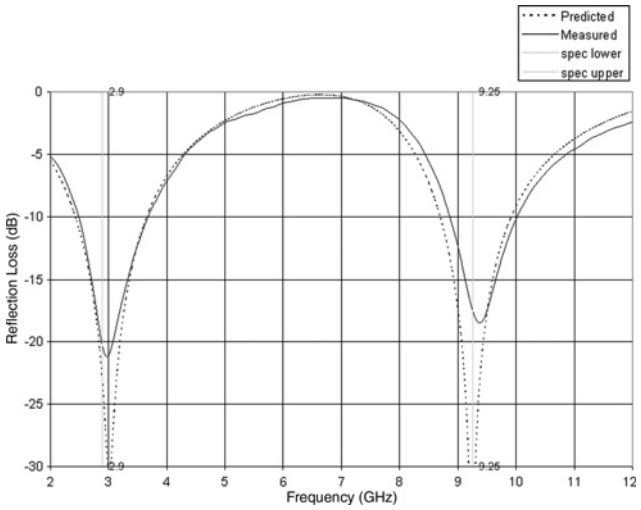

Figure 9 *Normal incidence performance of blade test panel*

The nacelle signature was addressed by the removal of the large vertical flat sides, which were divided into three regions. The same approach was taken as for the tower with sloping sides being selected to correspond to side-lobe minima in both bands. In the case of the V82, this corresponded to a slope angle of around 8°. A foil lining was added to prevent any scattering of energy from the generator inside the structure, this also having the benefit of reducing the level of any radiated emissions that might emanate from within the nacelle. Representations of the original and shaped nacelles are shown in Fig. 10.

Fig. 11 shows the corresponding effect on nacelle RCS derived using the MITRE PO code as a function of nacelle rotation (yaw) angle.

The RCS of the nosecone was substantially lower than other components (max ~17 dBsm). Hence this was unlikely to ever become the dominant scatterer. As such, apart from ensuring that the component was not transparent to microwave energy, no further treatment was deemed necessary.

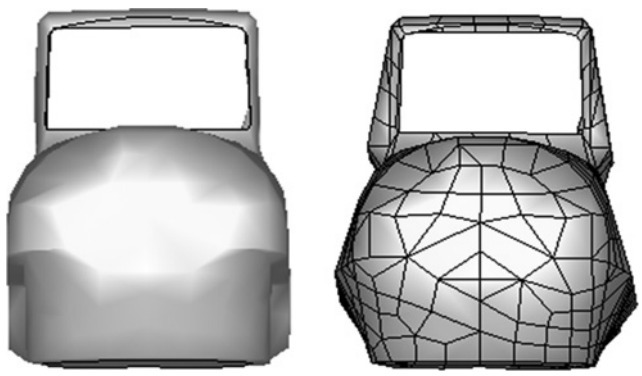

Figure 10 *Original (left) and shaped (right) nacelle for RCS reduction*

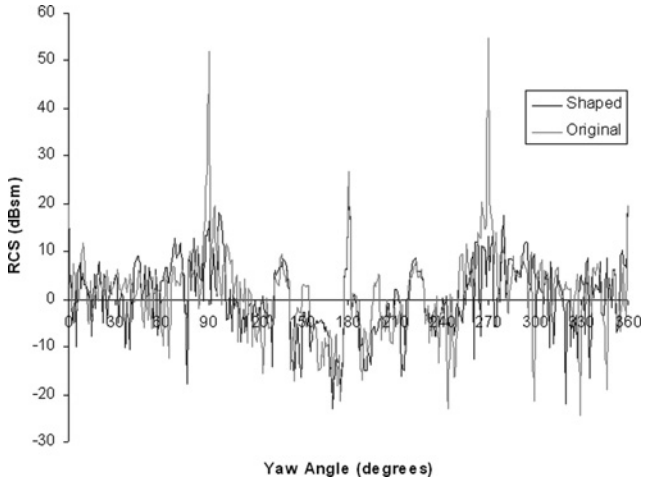

Figure 11 *RCS of nacelle before and after shaping at 3 GHz*

4 Radar impact modelling

Having derived estimates of the RCS of a 'treated' and 'untreated' turbine (the overall signature reduction is discussed in Section 5), the impact of the reduction achieved on radar performance was assessed by implementing a combined model, 'AEOLUS' [5]. AEOLUS uses the aspect-dependent RCS data for complete wind turbines derived from the MITRE PO code, propagation modelling originally developed for the prediction of TV and radio transmitter coverage [6] and a radar system model with typical parameters for AD and ATC radars. This system model is able, with terrain data, turbine type and knowledge of the layout of turbines within a proposed wind farm, to examine the effect of the wind farm on the ability of the radar to detect an air vehicle with a particular RCS in the vicinity of the farm. The code has served as an invaluable tool in the analysis of the effect of proposed wind farms and continues to be used in consultancy for wind farm developers and radar operators.

A case study based on the interaction of the Crystal Rig 2 wind farm (52 turbines, East Lothian, UK) with the Brizlee Wood radar was considered, this along with Crystal Rig I (25 turbines) formed the largest onshore farm at the time of study [7]. A 1 m^2 target was simulated flying various paths in the vicinity of, and then directly over, the wind farm at a range of 73 km from the radar with a bearing of 42° west of north. Far-field aspect-dependent RCS data were used in the prediction, although in practice the backscatter will be slightly reduced from the figures used because of the turbines being in the near field of the radiating aperture to some extent in the S-band. As the target approaches the wind farm detectability was found to be affected by the large returns from the wind farm. Specifically, these large returns significantly increase the constant false alarm rate-derived detection threshold in the vicinity of the farm.

Furthermore, assuming a 0 dBsm target directly illuminated by the main lobe of the radar antenna pattern and a +60 dBsm wind turbine illuminated by antenna elevation side lobes typically 30 dB down on the main lobe, consideration of the round trip losses suggests that the signal returned to the radar receiver is comparable in magnitude for both objects. Reduction of the wind turbine RCS by around 20 dBsm therefore leads to a comparable improvement in receiver signal to noise. A similar conclusion may be obtained from consideration of azimuth or range side lobes.

5 Summary

The application of shaping technology to the tower demonstrated that large reductions (>30 dBsm) in the RCS of this component are achievable with relatively trival changes at the design stage. An effective RAM was developed for the tower, although this was not considered feasible in light of other design requirements (environmental, mechanical, financial). Reductions of around 15 dBsm were achieved in both frequency bands of interest for the blades using a combination of Salisbury screen and CARAM-based designs. As with the tower, effective RAM designs were developed for the nacelle but shaping was the preferred method of signature reduction. By dividing the sides into three facets and increasing the slope angle, peak reductions of around 30 dBsm were achieved.

Fig. 12 shows the RCS of the V82 at 'boresight' before and after the use of the signature reduction techniques described for each component, as predicted using the MITRE PO code. The RCS for the case with the nacelle rotated through 90° (broadside illumination) is shown in Fig. 13.

Predictions and manufacturing trials suggest that significant reductions in turbine RCS can be achieved through the application of stealth technologies, and that the levels of reduction achieved, typically 30 dB for a turbine overall, are capable of bringing about real improvements in the ability of radars to detect air vehicles in the vicinity of wind farms. All the solutions developed

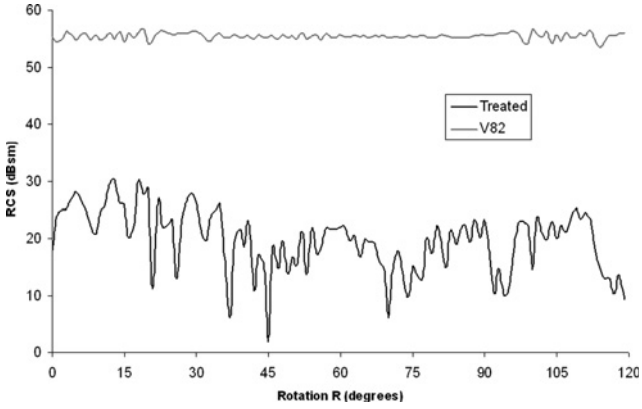

Figure 12 *V82 predicted RCS (0° yaw) with blade rotation angle, untreated against with stealth, 2.9 GHz*

IET Radar Sonar Navig., 2010, Vol. 4, Iss. 1, pp. 126–133
doi: 10.1049/iet-rsn.2009.0031

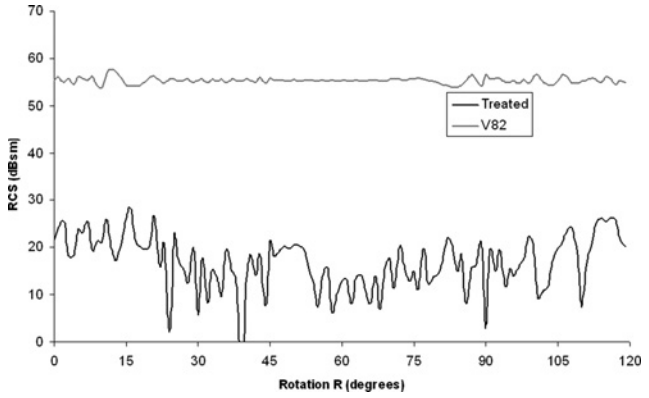

Figure 13 *V82 predicted RCS (90° yaw) with blade rotation angle, untreated against with stealth, 2.9 GHz*

were intended to address the environmental and mechanical requirements of the turbine components as well as achieving RCS budgets and hence be suitable for informing the development of future turbines. Likewise, the financial implications of the designs were also considered. Based predominantly on the materials and labour necessary for RCS reduction of the blades, it was estimated that the associated cost increase would be less than 10% of the current selling price of the turbine as a whole (this is currently estimated to be between £750K and £1M per MW).

6 Acknowledgment

The authors would like to thank all of the members of the Stealth Technology for Wind Turbines consortium including staff from BAE SYSTEMS ATC, the Universities of Manchester and Sheffield, the Turbine Manufacturer Vestas and the Department for Business Innovation and Skills (BIS).

7 References

[1] WOODS A.M., SILLENCE C.D., CARMODY K.D., *ET AL.*: 'Efficient radar cross section calculations on airframe geometries at high frequencies' (American Institute of Aeronautics and Astronautics, AIAA Test and Evaluation International Aerospace Forum, London, United Kingdom, 25–27 June 1996, 2nd edn.), Technical Papers (A96-31842 08-01)

[2] LORD J., MATTHEWS J.C.G., PINTO J.: 'RCS predictions for stealthy wind turbines'. EuCAP2006, Conf. Proc., 6–10 November 2006

[3] KNOTT E.F., SHAEFFER J.F., TULEY M.T.L.: 'Radar cross section' (Artech House, 1993, 2nd edn.), p. 549

[4] PINTO J., MATTHEWS J.C.G., SARNO C.: 'Radar signature reduction of wind turbines through the application of stealth technology'. European Conf. Antennas and Propagation, 23–27 March 2009, pp. 3886–3890

[5] MATTHEWS J.C.G., SARNO C., HERRING R.: 'Interaction between radar systems and wind farms'. Lougborough Antennas and Propagation Conf., 17–18 March 2008, pp. 461–464

[6] PREEDY K.A., TELFER C.R.: 'Software tools for the planning of VHF, UHF and microwave systems'. IEE, Sixth Int. Conf. Antennas and Propagation, ICAP 89 (Conf. Publ. No. 301), April 1989

[7] BWEA Press Release: http://www.bwea.com/media/news/ukwed.html

[8] http://www.theengineer.co.uk/Articles/311831/Renewables+recognition.htm

[9] http://www.bwea.com/pdf/AWG_Reference/0704_Marico%20BWEA_Radar.pdf

[10] PERRY J., BISS A.: 'Wind farm clutter mitigation in air surveillance radar', *IEEE Aerosp. Electron. Syst. Mag.*, 2007, **22**, (7), pp. 35–40

[11] TENNANT A., CHAMBERS B.: 'Signature management of radar returns from wind turbine generators', *Smart Mater. Struct.*, 2006, **15**, (2), pp. 468–472

[12] SERGEY L., HUBBARD O., DING Z., *ET AL.*: 'Advanced mitigating techniques to remove the effects of wind turbines and wind farms on primary surveillance radars'. IEEE Radar Conf., 2008, pp. 1–6

[13] GREVING G., BIERMANN W.: 'Application of the radar cross section RCS for objects on the ground – example of wind turbines'. Radar Symp., 2008, pp. 1–4